Computational Framework for Simulating Fluorescence Microscope Images With Cell Populations

Antti Lehmussola*, Pekka Ruusuvuori, Jyrki Selinummi, Heikki Huttunen, and Olli Yli-Harja

***Abstract*—Fluorescence microscopy combined with digital imaging constructs a basic platform for numerous biomedical studies in the field of cellular imaging. As the studies relying on analysis of digital images have become popular, the validation of image processing methods used in automated image cytometry has become an important topic. Especially, the need for efficient validation has arisen from emerging high-throughput microscopy systems where manual validation is impractical. We present a simulation platform for generating synthetic images of fluorescence-stained cell populations with realistic properties. Moreover, we show that the synthetic images enable the validation of analysis methods for automated image cytometry and comparison of their performance. Finally, we suggest additional usage scenarios for the simulator. The presented simulation framework, with several user-controllable parameters, forms a versatile tool for many kinds of validation tasks, and is freely available at http://www.cs.tut.fi/sgn/csb/simcep.**

***Index Terms*—Biomedical image processing, biomedical microscopy, simulation.**

I. Introduction

DUE to the advances in digital imaging technology, digital cameras are increasingly used in connection with optical microscopes. The use of digital imaging offers many unique attributes when comparing with the traditional microscopy, enabling automated analysis and efficient storage, without any technician-based error sources. Essentially, the advances in digital imaging have added momentum to the development in the field of automated image cytometry; that is, automated analysis of various cell-level properties from microscope images. Especially, a need for the automated analysis has raised from recently introduced high-throughput microscopy systems [1]–[3]. Without automated and efficient image analysis, the full potential of high-throughput microscopy can never be exploited.

In automated image cytometry, efficient and quantitative analysis is enabled by digital image processing. Commonly, the analysis proceeds as follows. First, the images obtained from a microscope are preprocessed in order to eliminate the errors originating from the measurement system, such as uneven illumination, detector noise, and compression artifacts. Second, the objects of interest, e.g., nuclei, cytoplasm, or some subcellular components, are extracted from the image. Finally, different features are quantified from the extracted objects and stored for further analysis. However, to be able to serve as a reliable source of information, all the analysis steps require accurate methods. Thus, the validation of analysis methods is an important part of any study utilizing automated image cytometry. A common approach for validation is to manually analyze the image, and then compare the results with the automatically obtained ones. Nevertheless, the repeatability of manual analysis can always be questioned due to technician-based error sources [4]. Moreover, in case of high-throughput microscopy systems, the validation by manual analysis becomes unrealistic due to the huge amount of available data.

In this study, we explore the use of image simulation in connection with the validation of analysis methods in automated image cytometry. With simulated images, the validation can be carried out more efficiently due to the available ground-truth information. More importantly, simulation allows validation with such a large amount of data not reasonable to achieve with real experiments. In this study, we aim at emulating the characteristics of the overall measurement system used in a typical fluorescence microscopy experiment. The simulation focuses on traditional wide-field fluorescence microscopy instead of confocal microscopy, since the benefits of simulation emerge best in connection with high-throughput microscopy, where confocal microscopy is a less common imaging modality. We propose that an easily adjustable simulation framework would provide an efficient tool to be used in connection with the applications of fluorescence microscopy, and especially in the validation of analysis methods. Previously, some studies have utilized simulation when developing algorithms for the automated analysis of microscopy images. However, the used simulation methods are often very simplified. For example, in [5] and [6], simplistic simulation was used when developing methods for confocal microscopy. In [5], only spheres, disks, and ellipsoids were used as simulated objects, and in [6], the objects were generated manually by hand. In [7], randomly located spheres were simulated when measuring the performance of 3D-FISH spot-counting algorithms. In our study, we aim at generating more extensive and controllable simulation framework than the previously presented ones, and emphasizing the usability of simulation in high-throughput microscopy.

Manuscript received October 16, 2006; revised March 15, 2007. This work was supported in part by the Academy of Finland (application number 213462, Finnish Programme for Centres of Excellence in Research 2006-2011) and in part by Tampere Graduate School, Information Science and Engineering (TISE). *Asterisk indicates corresponding author.*

*A. Lehmussola is with the Institute of Signal Processing, Tampere University of Technology, FI-33101 Tampere, Finland.

P. Ruusuvuori, J. Selinummi, H. Huttunen, and O. Yli-Harja are with the Institute of Signal Processing, Tampere University of Technology, FI-33101 Tampere, Finland.

Digital Object Identifier 10.1109/TMI.2007.896925

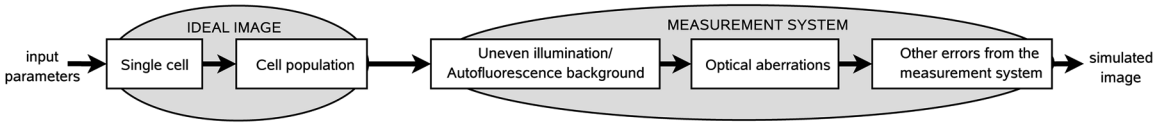

Fig. 1. Block diagram for the simulation. The simulation framework is based on different steps involved in generation of typical fluorescent microscope image. The ideal image is degraded progressively by different error sources originating from the image acquisition.

This paper is an extension of a previous study [8], where we introduced a prototype of our simulator. We extend the set of features described in the previous study by presenting a more realistic model for the optical system, more error sources, and a more sophisticated control of the spatial cell locations.

As the decades of continuous research in computer graphics demonstrate, the generation of synthetic images with real-life properties is a highly complex, and still unresolved task. However, the simplifications made when omitting some real world details allow us to concentrate on the essential features of the measurement system having the most straightforward effect on the performance of various analysis methods. Moreover, simplification is needed when simulating such complex biological objects as cells, having wide variety of different types with significantly differing characteristics. Such versatility in objects sets the requirement of a highly modifiable simulating methodology.

The rest of the paper is organized as follows. First, in Section II, we describe the proposed simulation framework in successive stages. The simulation process starts from the generation of an ideal microscope image consisting of desired cell population, and proceeds by degrading the ideal image with typical errors arising from the measurement system. All necessary source codes for simulation methods presented in this paper are made freely available. Thereafter, in Section III, we demonstrate the usefulness of simulation by validating the analysis results and comparing the performance of four tools for automated image cytometry. Finally, in Section IV, concluding remarks and other possible usage scenarios are given. Since the current article considers image simulation, the significance of visual examples can not be disputed. However, due to large resolution required for making all details of simulated images visible, it is not reasonable for us to present vast amount of example images here. Thus, we have made a companion website for this paper available.[1] This website offers a more extensive set of examples, and serves as a source-code repository for the simulation tool.

II. Simulation Methods

In our simulation methodology, the image formation is separated into successive stages involved in the image acquisition of a typical fluorescence microscopy experiment. First, an ideal image of the synthetic experiment is generated. The ideal image consists of the desired population of fluorescently labeled cells, excluding all error sources originating from the measurement system. This image and the underlying parameters serve as the ground-truth when validating various image processing algorithms for automated image cytometry. Thereafter, the ideal image is degraded by the errors arising from the measurement system. Finally, as an output of the simulation, an image of a synthetic experiment is obtained, sharing analogous properties with the real fluorescence microscope images. With versatile control over simulation parameters, simulated images with varying characteristics can be generated. In Fig. 1, the pipeline of the proposed simulation process is presented.

A. Single Cell

Single cells can be considered as the basic components of simulated microscope images. Commonly, most studies in traditional fluorescent light microscopy concentrate in objects such as whole cell, nucleus, cytoplasm, or subcellular components. For this reason, the accuracy of staining in our single cell model is restricted to these basic components. Similarly, as in real microscopy, different staining can be simultaneously used for different components, resulting as a multichannel representation of the simulated cell.

Consider the visual appearance of cells in a microscope image. Presumably, one of the most evident visual properties of single cells or cell organelles is the morphology. In addition, cell morphology often accompanies from various intracellular activities. Therefore, it is logical to initiate the simulation process by defining the shape for each individual cell. To the best of our knowledge, no extensive and accurate models for generating realistic cell shapes have been proposed in the literature. More importantly, enormous amount of shapes originating from various cell types or experimental conditions makes it unrealistic to cover all possible shapes in our simulation, whereas concentration into some specific cell type would limit the usability of simulation excessively. Nevertheless, due to the modular and freely available source-code, any additional shape models can be implemented in the simulator.

In the current study, we use a parametric model for the shape simulation. With the random model, a large scale of varying shapes can be obtained, enabling extensive testing of the object detection properties of different analysis algorithms. The random shapes are based on the parametric form of a circle, whose coordinates $(x(\theta), y(\theta))$ are described by

$$\begin{aligned} x(\theta) &= \cos(\theta) \\ y(\theta) &= \sin(\theta) \end{aligned} \tag{1}$$

where $\theta \in [0, 2\pi]$ is the polar angle. The shape is obtained through random polygons generated with (1). First, a regular polygon with k vertices is generated with equidistant sampling of angles θ. Thereafter, the spatial locations of the polygon vertices are randomized. The vertices of a random polygon with scale r, generated using a uniform distribution are defined as

$$\begin{aligned} x_i(\theta_i) &= r[U(-\alpha, \alpha) + \cos(\theta_i + U(-\beta, \beta))] \\ y_i(\theta_i) &= r[U(-\alpha, \alpha) + \sin(\theta_i + U(-\beta, \beta))] \end{aligned} \tag{2}$$

[1] http://www.cs.tut.fi/sgn/csb/simcep/

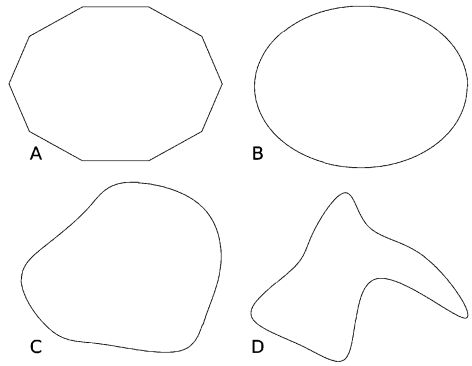

Fig. 2. Generation of random shapes with the parametric model. (A) A polygon without any randomness, and (B) the shape obtained when the vertices are connected with spline interpolation. More irregular shapes are obtained when the polygon vertices are dislocated using (2). (C) An example of a faintly irregular shape, and (D) clearly more distorted shape. Generally, irregular shapes are more typical to cell cytoplasm than nuclei.

for $i = 1, \ldots, k$, where $U(a, b)$ is a uniform distribution on the interval $[a, b]$. Now the parameter β controls the randomness of sampling, and α controls the randomness of the radius for the circle. Finally, the vertices are connected using cubic spline interpolation [9] which provides a smooth and flexible contour for the random shapes. In Fig. 2, the generation of random shapes is demonstrated visually. Fig. 2(a) illustrates a polygon without randomness ($\alpha = \beta = 0$) which generates a circular contour with spline interpolation in Fig. 2(b). In Fig. 2(c) and (d), it is demonstrated how increase in the scale of uniform distribution makes shapes more random. With different parameter combinations, the same shape model can be used for producing nuclei, cytoplasm, or some subcellular components.

Like the shape, the texture of cells can reveal relevant information on cell activity. Thus, texture analysis has been an active field of research in image cytometry (see, e.g., [10] and [11]). In fluorescence microscopy, the cell texture is a result of molecules emitting fluorescent light from either staining or autofluorescence of the studied cells. In the current study, we utilize a well-known procedural texture model [12] for synthesizing texture for simulated cells or cell organelles. The synthesized texture t in location (x, y) is defined as

$$t(x, y) = B + \sum_{i=0}^{n-1} p^i \eta_{xy}(2^i) \tag{3}$$

where a weighted sum of n octaves of basic noise function $\eta_{xy}(\cdot)$, producing noise with given frequency, is calculated. The scaling of noise functions is controlled with the persistence parameter p, and the bias with B. By controlling the parameters of the texture model, characteristics of the cell texture can be modified in a versatile way. When considering the validation of texture analysis algorithms in image cytometry, the property of generating textures with varying characteristics is essential. Again, when necessary, additional texture models can be implemented in the simulator.

B. Population of Cells

After defining the properties of single cells, it is natural to consider the global attributes of simulated images. Visually, the most obvious properties in this level are the number and spatial locations of the cells. Whereas the quantity of cells can be given as an unambiguous user-definable parameter N, specification of spatial cell locations is slightly more complex. The concept of cell locations can be studied in two perspectives: either as the spatial location in the whole microscope image, or as the mutual location of a cell compared with the others. In real microscope experiments, the specific location of a cell can occur due to different causes from randomness to biologically meaningful reasons like cell migration [13].

In our simulation, the cells are organized randomly. The spatial locations of cells seldom follow plain uniform distribution, since due to various biological reasons, the cells can appear e.g., in clusters in cell populations [14]. First, the number of cell clusters N_c is defined by the user, and subsequently the locations of the cell clusters (x_c, y_c) are distributed uniformly in the image. Thereafter, each simulated cell is either placed on the image based on a uniform distribution, or with probability p_c the cell is assigned in some of the clusters. The cells assigned into clusters, are organized randomly around the cluster centers according to a normal distribution. As a result, with probability $1 - p_c$ the spatial coordinates (x, y) of a cell are defined as

$$\begin{aligned} x &= U(0, d_x) \\ y &= U(0, d_y) \end{aligned} \tag{4}$$

where d_x, d_y are dimensions of the image. With probability p_c the coordinates are defined as

$$\begin{aligned} x &= x_c + N\left(0, \sigma_c^2\right) \\ y &= y_c + N\left(0, \sigma_c^2\right) \end{aligned} \tag{5}$$

where $N(0, \sigma_c^2)$ is a zero mean normal distribution with variance σ_c^2.

In the microscope images of cell populations, the cells are often spatially tightly packed or overlapping with each other. While developing methods for automated image cytometry, overlapping can be a significant problem since the overlapping cells cause errors in the analysis results. Thus, several attempts have been made for automatically separating overlapping cells [15], [16]. It is essential to control the overlapping also in the simulation. When considering the region of pixels R_i defined by a simulated cell, the relative amount of overlap L_{ij} caused by the region of pixels R_j of another cell can be measured by

$$L_{ij} = \frac{|R_i \cap R_j|}{|R_i|}, \quad i \neq j \tag{6}$$

where the operator $|\cdot|$ is the cardinality of a set. The maximum amount of allowed overlap is controlled with parameter $L_{\max}$. For example, when $L_{\max} = 1$ the overlapping is not limited in any way, and when $L_{\max} = 0$, no overlapping is allowed. If overlapping criterion is not satisfied, new coordinates for the simulated cell are generated.

C. Measurement System

The final step in the simulation degrades the previously obtained ideal image by several ways in a manner that resembles

the degradation caused by the real measurement system. In fluorescence microscopy, the measured image is a projection of the measured object corrupted by the defects in sample preparation and staining, unideal lighting and optical system, and noise of the detector. Despite the continuous improvements of the detectors and optical systems in microscopy, an ideal error-free measurement system can not be achieved. To emulate the image acquisition process, we implement error sources in our simulator resembling the background autofluorescence, nonuniform illumination, optical aberrations, and errors caused by the detector.

In an error-free measurement system, all information would originate only from the cells emitting fluorescent light. However, background intensity caused by autofluorescence and nonuniform illumination generate additional artifacts in the image. Nonuniform illumination of a microscope often causes a varying bias field to the image background. This results, for example, from a misaligned lamp, and is a common problem in the segmentation of biological images. As opposed to the background correction, which can be performed by fitting a two-dimensional polynomial to the original image, we simulate the nonuniform illumination by adding a second degree parabolic polynomial in the image. The center of the simulated illumination source is defined as vertical and horizontal misalignment (m_v, m_h) from the image center, and the energy of illumination source is controlled with parameter E_m. Finally, the autofluorescence effect, with energy E_a can be simulated as a spatially slowly changing random texture using (3).

Considering the samples used in fluorescence microscopy, it is a well-known fact that the thickness of the sample layer causes blurring to some of the objects [17], [18]. The blurring originates simply from the three-dimensional nature of the sample; only flat objects on a focal plane can be thoroughly in focus [19]. In addition, the further the objects are from the focal plane, the more blurred is their appearance. For generating spatially varying degradation, we define the point spread function (PSF) individually for each pixel. Since a spatially varying blurring kernel is required, traditional convolution is not valid for generating the blurring effect. Instead, we blur the images by a linear space-variant blur model [20], which defines the point spread function as a mapping of an impulse in location (p, q) into its neighborhood (x, y) with function $\mathrm{PSF}(x, y; p, q)$. In order to meet the demand for space-variant blurring and to link together the optics and distance based blurring effects, we approximate the point spread function with a Gaussian function. Thus, the point spread function centered at location (p, q) mapping an impulse into location (x, y) is given by

$$\mathrm{PSF}(x, y; p, q) = \exp\left(-\frac{0.5}{\sigma_g^2(p,q)}((x-p)^2 + (y-q)^2)\right) \quad (7)$$

where the amount of blurring is controlled with the variance $\sigma_g^2(p, q)$ of Gaussian kernel. The blurring effect controlled with σ_g^2 for each pixel location (p, q) is combined with the synthesis of cell shapes in order to create realistic appearance of cells both in and out of focus, and synthesis of background to emulate the effect of smoothly changing focus.

Finally, we add the error caused by the detector. Commonly, charge coupled device (CCD) detectors are used in microscopic imaging. The detector noise can be approximated by additive zero-mean Gaussian noise with variance σ_d^2 [20] denoted here by N_g. Herewith, the simulated image degraded by the image acquisition system $(\hat{I})$ becomes

$$\hat{I}(x, y) = \sum_{p,q \in R} \mathrm{PSF}(x, y; p, q) I(p, q) + N_g \quad (8)$$

where I is the ideal image with background originating from autofluorescence and uneven illumination, (x, y) and (p, q) are pixel locations, and R is a set of pixels around the specified pixel, in other words the support area for the point spread function. Fig. 3 demonstrates the visual appearance of space-variant blurring. It can be seen how the appearance of the uppermost cell is less blurred than the lower ones which are located farther from the focal plane.

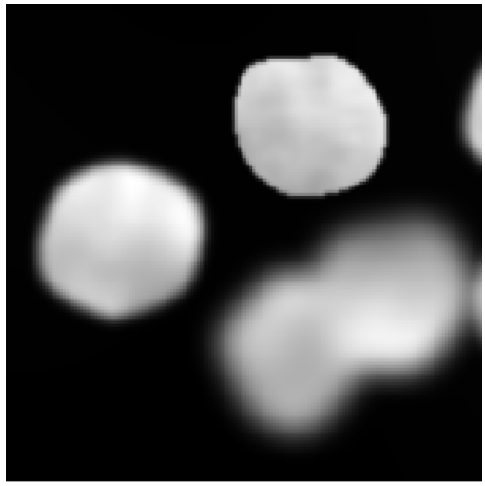

Fig. 3. Demonstration of space-variant blurring with a group of simulated cells. The topmost cell is located nearest to the focal-plane, and the two adjoint cells in the lower-right corner are farthest away from the focal-plane. The figure shows how the distance from the focal-plane results as a more blurred appearance.

Almost without an exception, measurement systems utilizing digital imaging, write the acquired image into an output file. Sometimes, due to large file sizes, the images are stored with lossy compression. Similarly as the optical system, the use of lossy compression generates artifacts in the image which need to be taken into account in our simulation. In general, the amount and severeness of the compression artifacts depend on the used compression efficiency, and the nature of the errors depend heavily on the used compression algorithm. Perhaps the most popular format for lossy compression is provided by JPEG standard [21], [22]. Therefore, the errors originating from image compression are simulated with JPEG compression. First, the compression introduces artifacts in high-frequency parts of the image. Second, since the compression is done in different color space, bleeding between color channels can occur. In case of fluorescence microscopy, the bleeding between color channels is especially considerable since different color channels should contain only information about some specific staining. In our simulation, the level of compression artifacts is controlled with parameter z defined as

$$z = 1 - Q \quad (9)$$

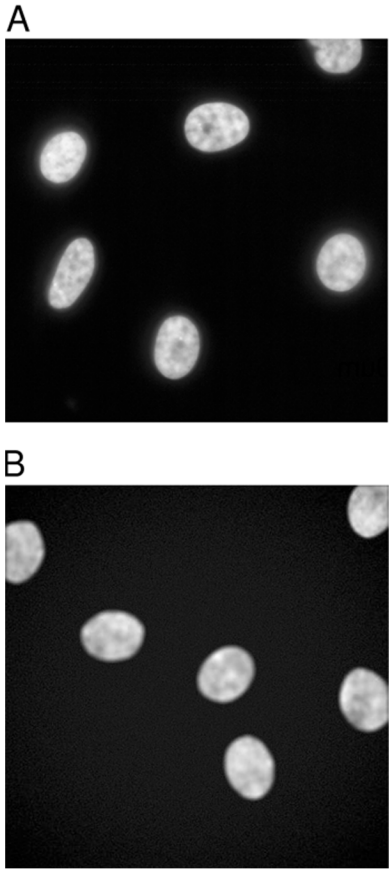

Fig. 4. Comparison of (A) real experiment with fluorescently labeled nuclei and (B) simulated image. Both images share very similar characteristics.

where Q is the efficiency of the compression, $Q \in [0,1]$, in JPEG compression. The resulting simulated image compressed according to z is given as

$$I_s = C(\hat{I}, z) \tag{10}$$

where $\hat{I}$ is an image of the form given in (8) and C is the function for JPEG compression. A more detailed view on JPEG compression can be obtained from the literature [21], [22].

In Fig. 4, the resemblance in close-ups of simulated image I_s and real fluorescently labeled nuclei is demonstrated. When comparing the images visually, both images share very similar properties.

In case of validation, the properties of the presented simulation framework provide the most significant advantage in connection with high throughput microscopy. Therefore, the simulation can also be used for generating high-throughput cell array experiments [1], where the experiment consists of several spots of different cell populations. Fig. 5 demonstrates a simulated cell array experiment generated using the presented simulation methods.

D. Simulation Tool

The proposed simulation methodology is developed as a software package called SIMCEP implemented with Matlab (MathWorks, Natick, MA). The source-codes of the software are freely available from the companion website under the terms of GNU general public license. The motivation behind the software is to allow a hands-on experience on the simulation methods presented in this paper. Furthermore, the software will provide a modular tool for future research. Since the source codes for the simulation methods are freely available for modification, the functionality of the simulator can be extended. For example, depending on application, it is possible to implement additional models for shape or texture simulation. A more detailed documentation of the usage is available from the companion website.

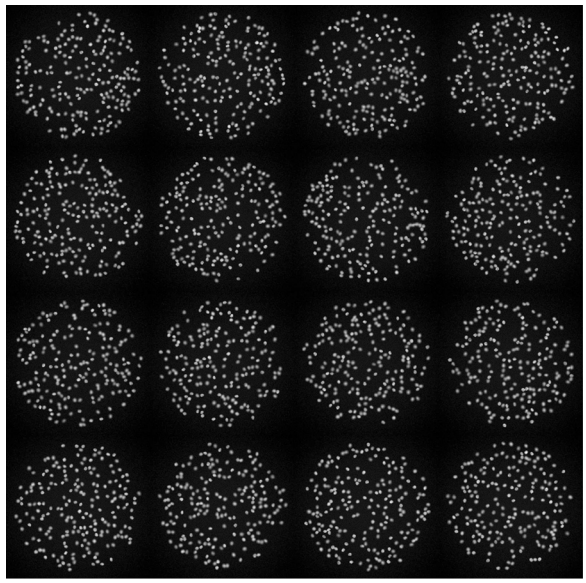

Fig. 5. Simulated cell array experiment consisting of 16 spots. In high-throughput microscopy systems, such as cell arrays, the validation of analysis results is extremely laborious without simulation.

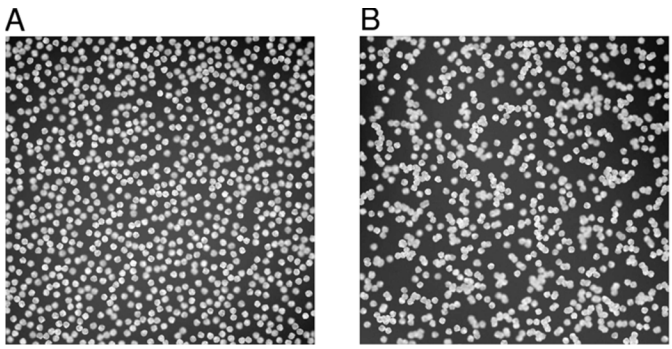

Fig. 6. Two example images used when comparing performances of different analysis tools. (A) Simulated image without almost any overlapping objects. (B) Simulated image with many objects clearly overlapping with each other. In our experiment, the largest performance differences between tools originated from overlapping objects.

III. Validation Case Study

In this section, we demonstrate the usability of the proposed simulation framework in the validation of different analysis methods. Commonly, the results of automated image cytometry algorithms are validated by comparing analysis results with ground-truth established by manual analysis (see e.g., [23]–[25]). Manual analysis, however, is time consuming, very tedious, and the results suffer from variability between

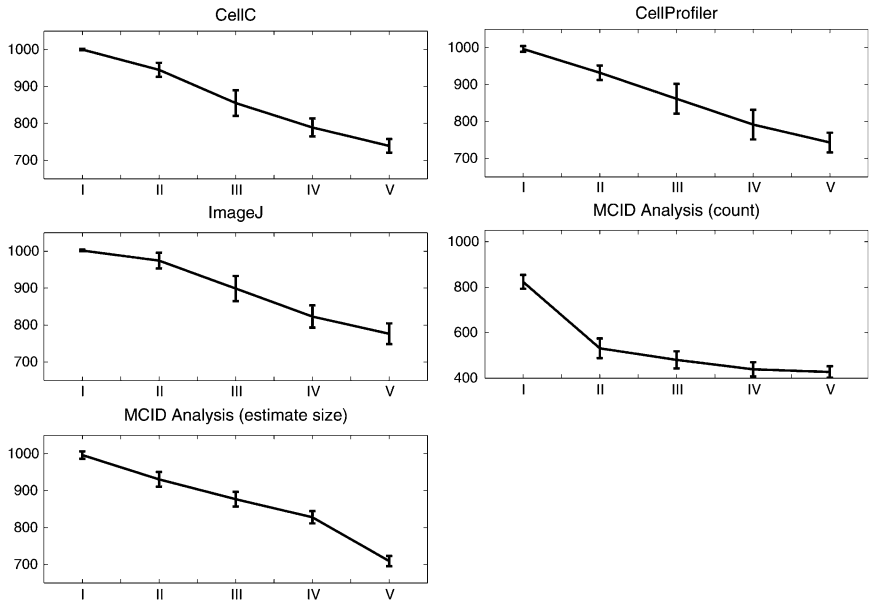

Fig. 7. Results for validation case study, where each analyzed image contained 1000 cells. The graph presents the medians of obtained analysis results (number of cells) within each set of ten images, including error bars two standard deviations in length. As the overlapping increases from set I to V, the performance of analysis tools clearly decreases. Notice that the scale in MCID analysis (count) is different than in other tools.

the observers. Moreover, the larger the set of images under manual analysis, the higher the variability will be. Therefore, the manual validation becomes impractical especially in the case of high-throughput microscopy.

For our validation test case, we selected four tools developed for automated image cytometry: CellC v1.11 [26], ImageJ v1.36b [27], CellProfiler [28], and MCID Analysis (Imaging Research Inc., Catharines, ON, Canada; Evaluation ver. 7.0). Using simulated test images, we measured how accurately each tool performs cell enumeration. To justify the use of simulation, we aimed at generating such an extensive set of test images which is not reasonable to be analyzed manually. Altogether, we generated five sets (I-V) of ten images (overall 50 images), where each image consisted of 1000 cells. After each ten image set, the allowed overlapping between adjacent cells was increased gradually. In Fig. 6, examples of simulated images are presented. Finally, the simulated images were analyzed with each tool and the analysis results were compared with the ground-truth. For MCID Analysis, we used two different analysis methods. A method where the number of objects was calculated without extracting overlapping objects from each other, and a method where the number of objects was estimated using overall segmented area and presumed object size. More detailed description of analysis parameters used in each tool is available at the companion web page.

The number of cells obtained with different analysis tools is presented in Fig. 7. For each tool, the graph presents the medians of obtained analysis results within each set of ten images, including error bars two standard deviations in length. The results show that as the overlap increases, the performance of each analysis tool decreases. Clearly, the worst results are obtained with MCID Analysis when only the number of segmented objects are calculated. CellC, ImageJ, and CellProfiler all include method for separating overlapping objects, and, therefore, their results are more competitive. However, as the overlapping increases the performance of separation also clearly decreases. MCID Analysis with object-size-based estimation gives rather accurate results, which can be expected since all simulated objects had very similar size. Based on the obtained results, we conclude that the presented simulation framework provides possibility to compare results obtained with various analysis tools against the ground truth information. More importantly, validation by simulation provides valuable information about the properties of analysis methods and facilitates the selection of suitable tools for different analyses.

IV. Discussion

This study presented a methodology for simulating the fluorescent microscope images of cell populations. We aimed at emulating the characteristics of the overall measurement system in a typical fluorescence microscope experiment. The simulation proceeds in stages typical for a fluorescence microscope experiment. First, a desired cell population is generated consisting of single cells with defined properties. Due to the possibility of multichannel imaging, different components of the cell can be simulated simultaneously. Thereafter, the resulting ideal image of the experiment is degraded by the influence of various error sources present in the measurement system. With the modifications of the simulation parameters, simulated images with wide variety of characteristics can be generated.

Perhaps the most unique attribute provided by the simulation is the availability of reliable ground-truth information. Without simulation, no similar ground-truth information is available, and, therefore, the validation of analysis methods is commonly performed manually. However, manual validation can be considered extremely laborious and prone to various errors. As demonstrated in Section III, by knowing the true properties of the images, the validation of cell enumeration methods can be

effectively performed. With our simulation, the performance of different analysis tools was studied under varying conditions, and clear differences between the tools were identified. Similar experiments could be also carried out for other image cytometry algorithms: For example, the validation of morphology or texture analysis methods could be potential applications. Especially, the use of simulation becomes extremely valuable in case of the emerging high-throughput microscopy, where the large amount of available data makes the manual validation totally unrealistic.

The proposed simulation framework has several additional applications. For example, in case of cell enumeration, manual counting is still also a very popular approach. Therefore, it would be very interesting to use our simulated images to measure how accurately a human observer can e.g., count the number of cells, and to compare how these results differ between individuals, and how error rate increases in case of a larger set of images or different viewing conditions. In addition, simulation is known as an efficient tool for education since it provides a realistic view of the studied phenomenon in a risk-free environment without any major financial costs. Therefore, the proposed simulation framework would allow the students to efficiently learn the cause and effect of their choices in fluorescence microscopy. Finally, since the output image of a fluorescence microscope is always distorted by optical aberrations and additive noise, the development of image restoration algorithms is an important field of research. Since the ideal image from a real optical system is impossible to obtain, the proposed simulation framework would provide ground truth information when measuring the performance of different restoration algorithms. When extending the simulation framework for other fluorescence microscopy based measurement systems, the amount of usage scenarios increases.

An interesting future direction would be to combine simulation of biological information with the current study. For example, gene-level activity can be linked with the changes in the appearance of cells (e.g., shape or texture). By using simulated gene regulatory networks, cells with specific activity could be simulated, providing a more biologically motivated simulation result. The same approach could also be used for generating subpopulations with realistically discriminating characteristics, and therefore allowing more diversity in the simulation results.

REFERENCES

[1] J. Ziauddin and D. M. Sabatini, "Microarrays of cells expressing defined cDNAs," *Nature*, vol. 411, pp. 107–110, 2001.

[2] S. Mousses, N. J. Caplen, R. Cornelison, D. Weaver, M. Basik, S. Hautaniemi, A. G. Elkahloun, R. A. Lotufo, A. Choudary, E. R. Dougherty, E. Suh, and O. Kallioniemi, "RNAi microarray analysis in cultured mammalian cells," *Genome Res.*, vol. 13, pp. 2341–2347, 2003.

[3] X. Zhou and S. Wong, "Informatics challenges of high-throughput microscopy," in *IEEE Signal Process. Mag.*, May 2006, vol. 23, no. 3, pp. 63–72.

[4] D. Webb, M. A. Hamilton, G. J. Harkin, S. Lawrence, A. K. Camper, and Z. Lewandowski, "Assessing technician effects when extracting quantities from microscope images," *J. Microbiol. Meth.*, vol. 53, pp. 97–106, 2003.

[5] S. J. Lockett, D. Sudar, C. T. Thompson, D. Pinkel, and J. W. Gray, "Efficient, interactive, and three-dimensional segmentation of cell nuclei in thick tissue sections," *Cytometry*, vol. 31, pp. 275–286, 1998.

[6] C. O. de Solórzano, E. G. Rodriguez, A. Jones, D. Pinkel, J. W. Gray, D. Sudar, and S. J. Lockett, "Segmentation of confocal microscope images of cell nuclei in thick tissue sections," *J. Microsc.*, vol. 193, pp. 212–226, 1999, (Pi3).

[7] A. M. Grigoryan, G. Hosteller, O. Kallioniemi, and E. R. Dougherty, "Simulation toolbox for 3D-FISH spol-counling algorilhms," *Real-Time Imag.*, vol. 8, pp. 203–212, 2002.

[8] A. Lehmussola, J. Selinummi, P. Ruusuvuori, A. Niemislö, and O. Yli-Harja, "Simulating fluorescenl microscope images of cell populations," in *Proc. 2005 IEEE Eng. Med. Biol. 27th Annu. Conf.*, 2005, pp. 950–953.

[9] M. Unser, "Splines: A perfect fit for signal and image processing," in *IEEE Signal Processing Mag.*, Nov. 1999, vol. 16, no. 6, pp. 22–38.

[10] M. Guillaud, K. Adler-Storthz, A. Malpica, G. Staerkel, J. Matisic, D. V. Niekirk, D. Cox, N. Poulin, M. Pollen, and C. Macaulay, "Subvisual chromatin changes in cervical epithelium measured by texture image analysis and correlated with HPV," *Gynecol. Oncol.*, vol. 99, pp. S16–S23, 2005.

[11] Y.-C. He, W. Peng, J.-G. Qiao, J. Cao, and J.-W. Chen, "Relationship between nuclear morphometry, DNA content and resectability of pancreatic cancer," *World J. Gastroenterol.*, vol. 9, pp. 1863–1865, 2003.

[12] K. Perlin, "An image synthesizer," *Comput. Graph.*, vol. 19, pp. 287–296, 1985.

[13] D. A. Lauffenburger and A. F. Horwitz, "Cell migration: A physically integrated molecular process," *Cell*, vol. 84, pp. 359–369, 1996.

[14] J. Kolega, "The movement of cell clusters in vitro: Morphology and directionality," *J. Cell Sci.*, vol. 49, pp. 15–32, 1981.

[15] C. G. Loukas and A. Linney, "A survey on histological image analysis-based assessment of three major biological factors influencing radiotherapy: Proliferation, hypoxia and vasculature," *Comput. Methods Programs Biomed.*, vol. 74, pp. 183–199, 2004.

[16] N. Malpica, C. O. de Solórzano, J. J. Vaquero, A. Santos, I. Vallcorba, J. M. García-Sagredo, and F. del Pozo, "Applying watershed algorithms to the segmentation of clustered nuclei," *Cytometry*, vol. 28, pp. 289–297, 1997.

[17] S. J. Lockett and B. Herman, "Automatic detection of clustered, fluorescent-stained nuclei by digital image-based cytometry," *Cytometry*, vol. 17, pp. 1–12, 1994.

[18] A. Dieterlen, C. Xu, M.-P. Gramain, O. Haeberle, B. Colicchio, C. Cudel, S. Jacquey, E. Ginglinger, G. Jung, and E. Jeandidier, "Validation of image processing tools for 3-d fluorescence microscopy," *C. R. Biol.*, vol. 325, pp. 326–334, 2002.

[19] H. Netten, I. T. Young, L. J. van Vliet, H. J. Tanke, H. Vroljik, and W. C. Sloos, "Fish and chips: Automation of fluorescent dot counting in interphase cell nuclei," *Cytometry*, vol. 28, pp. 1–10, 1997.

[20] H. Kaufman and M. Tekalp, "Survey of estimation techniques in image restoration," *IEEE Contr. Syst.*, vol. 11, no. 1, pp. 16–24, Jan. 1991.

[21] R. C. Gonzalez and R. E. Woods, *Digital Image Processing*, 2nd ed. Englewood Cliffs, New Jersey: Prentice-Hall, 2002.

[22] J. C. Russ, *The Image Processing Handbook*, 3rd ed. Boca Raton, FL: CRC Press, 2000.

[23] R. Gür, B. Guggenheim, E. Giertsen, and T. Thurnheer, "Automated immunofluorescence for enumeration of selected taxa in supragingival dental plaque," *Eur. J. Oral Sci.*, vol. 108, pp. 393–402, 2000.

[24] J. Pernthaler, A. Pernthaler, and R. Amann, "Automated enumeration of groups of marine picoplankton after fluorescence in situ hybridization," *Appl. Environ. Microbiol.*, vol. 69, pp. 2631–2637, 2003.

[25] R. Thiel and M. Blaut, "An improved method for the automated enumeration of fluorescently labelled bacteria in human faeces," *J. Microbiol. Methods*, vol. 61, pp. 369–379, 2005.

[26] J. Selinummi, J. Seppälä, O. Yli-Harja, and J. A. Puhakka, "Software for quantification of labeled bacteria from digital microscope images by automated image analysis," *Biotechniques*, vol. 39, pp. 859–863, 2005.

[27] M. D. Abramoff, P. J. Magelhaes, and S. J. Ram, "Image processing with ImageJ," *Biophotonics Int.*, vol. 11, pp. 36–42, 2004.

[28] A. E. Carpenter, T. R. Jones, M. R. Lamprecht, C. Clarke, I. H. Kang, O. Friman, D. A. Guertin, J. H. Chang, R. A. Lindquist, J. Moffat, P. Golland, and D. M. Sabatini, "Cellprofiler: Image analysis software for identifying and quantifying cell phenotypes," *Genome Biol.*, vol. 7, p. R100, 2006.